Journal of
Materials Chemistry C

REVIEW

View Article Online
View Journal | View Issue

Cite this: *J. Mater. Chem. C*, 2017, 5, 2758

Electromagnetic wave propagation in a rolled-up tubular microcavity

Gaoshan Huang[ab] and Yongfeng Mei*[a]

Received 17th January 2017,
Accepted 13th February 2017

DOI: 10.1039/c7tc00283a

rsc.li/materials-c

Strain-engineering of nanomembranes with pre-defined geometries leads to fabrication of microtubular structures by lift-off technology, which provide tunable three-dimensional confinement of electromagnetic waves propagating both in circular cross section and along the longitudinal direction (tube axis) as microscale resonators. By changing the rolling geometry and functional materials of rolled-up microcavities, manipulation of the electromagnetic waves in the microcavities has been demonstrated (*e.g.*, in the case of metamaterials and photonic crystals) and spin–orbit coupling was also observed recently. Moreover, the interactions of the electromagnetic waves with their environments have led to advantageous sensing applications of rolled-up microcavities such as molecule detection and opto-fluidic refractometry. This review will summarize recent experimental and theoretical progress concerning rolled-up tubular microcavities and focus on resonance tuning and sensing applications.

1 Introduction

In general, a resonator is a device that can oscillate at certain frequencies with greater amplitudes and is normally used to generate waves of certain frequencies or to select specific frequencies.[1] According to the nature of the oscillation, resonators are grouped into mechanical resonators and electromagnetic resonators. The demand for devices with small dimensions and high performance (*e.g.*, Moore's law) has stimulated intensive research and enormous progress in miniaturization of devices has been achieved. With the development of micro-/nano-fabrication techniques, researchers are now able to obtain resonators with different geometries on micro and even nano scales. Thus, on-chip integration of resonators with other components for micro-/nano-electromechanical systems and lab-on-a-chip applications is becoming feasible.[2–8] Electromagnetic resonators in the micrometer range normally have an interior space for the wave to propagate in, and therefore, are commonly called microcavities as well. Among the various

[a] *Department of Materials Science, Fudan University, Shanghai 200433, P. R. China. E-mail: yfm@fudan.edu.cn*
[b] *National Key Laboratory of Fundamental Science of Micro/Nano-Device and System Technology, Chongqing University, Chongqing 400030, P. R. China*

Gaoshan Huang

Gaoshan Huang received his PhD in condensed matter physics at Nanjing University, China, in 2007. After graduation, he worked at IFW Dresden, Germany as a guest scientist. Then he moved to IMRE, Singapore as a research engineer. In 2010, he joined the Department of Materials Science, Fudan University, China, as an associate professor. His current research interest is fabrication and characterization of low-dimensional structures.

Yongfeng Mei

Yongfeng Mei received his BS and MS in physics from Nanjing University and PhD in materials physics from City University of Hong Kong. He is a professor in the Department of Materials Science at Fudan University. Before that, he worked as a postdoctoral researcher in the Max Planck Institute for Solid State Research and then led a research group in the Leibniz Institute for Solid State and Materials Research Dresden as a staff scientist. His current research interest focuses on the development of inorganic nanomembranes and their properties in optics, opto-electronics, flexible electronics and micro-/nanoscale robotics.

microcavities with diverse morphologies that have been developed, four configurations have been proposed, each based on a different manner of confinement: first, the Fabry–Perot microcavity, where the wave oscillates between two reflectors;[9,10] second, the distributed feedback microcavity, which selectively reflects the wave;[11] third, the photonic crystal defect microcavity, where a defect mode is produced by breaking the periodic structure;[12,13] fourth, the whispering-gallery mode (WGM) microcavity, where a wave is confined by continuous total internal reflection.[10,11,14,15] Among all these microcavities, the WGM-type ones have attracted increasing focus and are extensively studied due to their advantages of high quality factor (Q-factor), low mode volume, and large optical density.[11,16,17]

The ''whispering gallery'' phenomenon was first systematically investigated more than 100 years ago by Rayleigh, who studied the acoustic wave propagation in the dome of St. Paul's Cathedral in London, UK.[18,19] The internal reflection of the wave at the curved wall, making the wave travel along the surface, was considered to be a new propagation mode.[18,19] This propagation mode (*i.e.*, WGM) was later to be extended into the electromagnetic wave regime, as suggested by Richtmyer in a spherical dielectric microstructure,[20] and then experimentally realized in 1961.[21] Motivated by these pioneering works, microcavities with WGM-type resonance have been successfully fabricated in microstructures with different geometries including sphere,[22–24] disk,[25] ring/toroid,[26–29] goblet,[30] peanut,[31] bottle,[32,33] and bubble[34,35] shapes. Their applications as filters,[36] light sources,[37] lasers,[38] *etc.* have been widely explored.[39] It is worth noting that WGM-type microcavities require wave reflection from the curved outer surface only,[17] and therefore the microstructures can be non-uniform, as in the case of microrings, which contain a hollow interior. For a hollow cavity with a thick wall (thickness $\gg$ wavelength), the distribution of the WGM should be similar to a filled cavity with the same dimensions. However, if the thickness of the wall approximates the wavelength, simulation indicates that a pronounced evanescent field should extend into the surrounding medium,[39] causing the microcavity to behave differently from the classic WGM resonator. The part of the mode located outside the wall of the hollow resonator in the form of the evanescent field will lead to a shift in the resonant wavelength if the surrounding medium is changed.[39] The change can be mathematically described by introducing a parameter – the effective refractive index n_{eff},[40] – and the shift can be calibrated for sensing applications.[11,39,41] As a three-dimensional (3D) hollow WGM resonator, a microtubular resonator has also been fabricated and investigated.[17] In contrast to its 2D counterpart (*i.e.*, microring resonator), the microtubular cavity combines resonance and fluidics and thus opto-fluidic devices can be produced.[42] Its integratability enables a label-free and/or real-time sensing of molecules in fluids.[39,43–46]

Tubular microcavities are normally made from glass capillaries and this material, composed of SiO_2, is also widely used in telecommunications.[24,39,45] Typically, the glass capillary is tapered down to the required diameter and the wall thickness may be further thinned by chemical etching. More complex geometries like bottle or bubble shapes have also been obtained by using gas pressure to push the wall after heating.[34,39] To expand the range of materials in microtubular cavities,[47–50] researchers have adopted rolled-up technology to fabricate microtubes by releasing pre-strained nanomembranes,[51–53] and the first report of using a rolled-up tube as a resonator was published in 2006.[55] As a rapidly developing area, many theoretical and experimental works have been published since then.[17,54]

In this review, we will focus on the recent progress in resonance tuning in rolled-up tubular microcavities. The features exclusively connected to the ''rolled'' geometry (*i.e.*, spiral cross section) and corresponding layered tube wall will be emphasized. The sensing applications of rolled-up tubular microcavities will also be summarized.

2 Electromagnetic wave confinement

Fig. 1(a) demonstrates an ordered array of microtubes fabricated by rolling pre-defined square-shape nanomembranes. These typical rolled-up tubes are uniform and aligned in the same direction, which is beneficial for on-chip integration (the details can be found in ref. 53). The emission and absorption characteristics of such rolled-up microtubes often demonstrate modulations in the visible range (Fig. 1(b)) and are commonly ascribed to optical resonance, which originates from the circulation and constructive interference of electromagnetic waves in the cross section.[55–61] Under a rough approximation, the rolled-up structure is considered as a normal tube with cylindrical symmetry and the cross section becomes a ring. This ring resonator may be further regarded as a planar waveguide with length (circumference of the ring) $l = \pi(R_o + R_i)$, where R_o and R_i are the outer and inner radii respectively. The resonant wavelength λ can be calculated by considering the periodic boundary condition $n_{\text{eff}}l = m\lambda$, where m is the azimuthal mode number.[55] However, due to the over-simplified model used here, the obtained resonant wavelengths may deviate greatly from the experimental results. In order to calculate the value more accurately, the spiral cross section should be taken into consideration, and three approaches to this have been proposed. The first approach starts from Maxwell's equations, setting up a Schrödinger-like wave equation, and solves the eigenvalue problem by using the boundary conditions obtained from Maxwell's equations.[55,62] The second approach uses the Mie scattering method to calculate the resonant wavelength.[63,64] In contrast to the first approach, this approach also has the ability to calculate the Q-factors of the modes. The third approach is numerical simulation using the finite-difference time-domain (FDTD) method or finite element method.[60,62,65,66] The intensity of the electrical field can be easily simulated (see the inset of Fig. 1(b)). Moreover, this approach is also capable of calculating the Q-factors, but normally at the cost of long computational times, especially for high Q cases.[63]

Detailed investigation demonstrates that in the spiral structure, the edges of the nanomembrane (both starting and ending edges, known as notches), and the corresponding broken cylindrical symmetry, allow the degenerate mode in the ring structure to

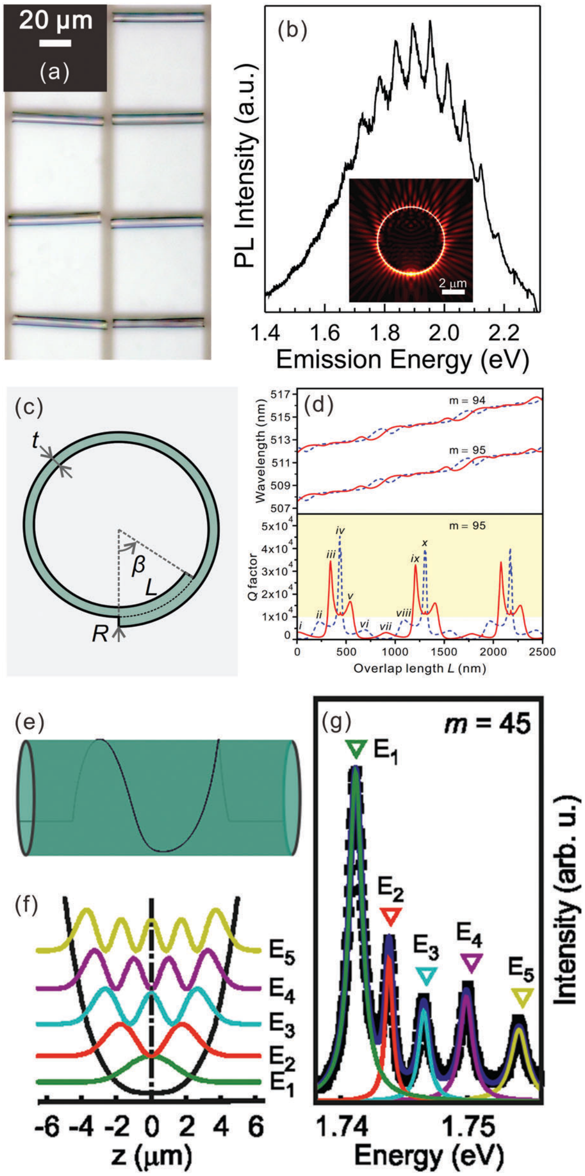

Fig. 1 (a) Optical microscope image of microtubular array fabricated by rolling square nanomembranes. Adapted from ref. 60, with the permission of AIP Publishing. (b) Typical photoluminescence spectrum from a microtubular resonator. The inset shows the intensity pattern of the resonant electric field obtained from FDTD simulation. Adapted from ref. 60, with the permission of AIP Publishing. (c) A rolled-up microtube with overlap length L. (d) Evolution of resonant wavelengths (upper panel, azimuthal number m = 94 and 95) and Q-factor (lower panel, azimuthal number m = 95) as a function of overlap length L. Roman numerals in lower panel mark the first ten local maxima of the Q-factors. (c) and (d) are adapted with permission from ref. 67. Copyright 2016 by the American Physical Society. (e) Illustration of the lobe structure, which results in the axial confinement. (f) Calculated axial potential (black line) and the first five axial fields (colored lines) corresponding to the axial confinement. (g) Photoluminescence spectrum at the middle of the lobe. The black points are experimental data, the solid colored lines are Lorentzian fitting of the individual modes, and the inverted triangles correspond to calculated energies using the axial confinement model. (e–g) are reprinted from ref. 72, with the permission of AIP Publishing.

be separated into two modes.[66] The two modes have different field distributions and circulation lengths, resulting in slightly different resonant wavelengths.[66] Fang *et al.*[67] further disclosed that the chirality of the spiral cross section and the overlap (with length L) (Fig. 1(c)) between the two notches cause a shift of the resonant wavelengths of both modes, as illustrated in the upper panel of Fig. 1(d).[67] An obvious modulation of the Q-factors of the two modes (lower panel in Fig. 1(d)) is also evident. Detailed analysis shows that the local maximum of the Q-factor is obtained when the splitting between the resonant wavelengths of the two modes is nearly zero.[67] This is a typical feature of open or dissipative systems,[68,69] and is considered to be due to the strong resonant interactions between the inner and outer notches *via* scattered waves within the overlap area.[67] In the case of a thicker wall with many tube rotations, the confinement of the field within the wall is improved while the change in thickness at the notches is reduced, and thus the splitting becomes negligible.[66]

Since the rolled-up microtube is a 3D structure, it cannot be fully understood on the basis of its 2D cross section alone. The 3D geometry will influence the resonance performance in two respects. First, as the geometry of the "ring" significantly influences the resonance,[55] the resonances are different even at different positions along the axis.[59] This is because the rolling is a self-assembly process which cannot produce a perfectly uniform cross section along the tube axis. The fluctuation in the shape, the diameter, and the number of rotations (which is generally not an integer) will be reflected in the shift of the resonant wavelength. Second, due to the propagation of the electromagnetic wave along an axis direction with limited length, confinement of the wave in this direction also produces fine resonance.[58] A series of sub-peaks, henceforth known as axial modes, have been observed in the spectral characterization of microtubes.[58,64,70,71] The phenomenon was first reported in rolled-up microtubes with intentionally designed rolling edges (also known as lobes) with circular, parabolic, triangular, and rectangular shapes.[58,64] An analytical method based on the adiabatic approximation was adopted to solve this 3D confinement, where the circular propagation in the cross section and the axial propagation were separated for the sake of simplicity.[58] For a typical resonator, as shown in Fig. 1(e), the axial potential energy curve induced by the edge of the nanomembrane is plotted in Fig. 1(f). The calculated axial modes in Fig. 1(f) are in good agreement with those observed in experiments (Fig. 1(g)).[72] In addition, as shown in Fig. 1(f), the distribution of the axial modes varies along the axis. This dependence can be exploited to tune the resonance or extract specific information.[72] In addition, axial confinement can also be intentionally introduced by producing microtubes with artificial structures, as reported in ref. 47, 69, and 73, where systematic theoretical (both analytical and numerical) and experimental investigations on 3D wave confinement were presented.

Here, in the last part of this section, we should stress that WGM is not the only approach to confinement of the wave in microtubular structures. In our recent work, we investigated the propagation of infrared waves in a rolled-up microtube by using numerical simulation based on the finite element method, and no obvious WGM could be observed in the tube wall.[74]

This is believed to be due to the thinness of the wall ($\sim$210 nm) compared to the wavelength, as a result of which the wave could not be confined. However, the wave could be trapped in a hollow core as a result of repeated reflection at the inner surface of the tube wall, which also promotes the interaction between the wave and the material.[74] This approach hints at a great potential for photodetection by using 3D rolled-up devices.

3 Asymmetric geometries and resonance tuning

It is worth noting that in real experimental work, the rolled-up microtubes are more or less asymmetric – the tubes are cone-like. To investigate this in detail, Bolaños Quiñones *et al.*[75] intentionally prepared a cone-like tube with a diameter difference of around 1 μm, and investigated the resonance both theoretically and experimentally. The axial potential in this tube had a minimum near the larger side, in contrast to that in an ideally symmetrical tube (Fig. 1(f)). The corresponding axial modes had a larger energy spacing, due to the enhanced axial confinement with a narrower and deeper potential well.[75] The conical degree and the length of the tube both influenced the axial confinement, leading to an obvious shift of the axial modes. A detailed description of the calculation and simulation of resonance in asymmetrical microtubular resonators can be found in a recently published work.[76]

Besides the geometrical parameters of the microtubular resonator, the resonant wavelength can also be tuned by a coupling between the resonator and nearby objects *via* the evanescent field. Researchers have introduced luminescent nanoparticles into microtubular resonators after the rolling process, and an obvious coupling effect is noticed: resonance is observed in the emission range of the nanoparticles.[73,77] By depositing the nanoparticles onto the nanomembranes before the rolling process, researchers have embedded the nanoparticles between the windings of the tube wall to achieve a more efficient coupling.[78] A suitable choice of nanoparticles was found to be able to tune the resonant wavelength across quite a large range.[78] Moreover, it was reported that the aggregated nanoparticles (or quantum dots) could act not only as a light source but also had the potential to provide additional confinement in the axial direction, thus providing another way to tune the resonance.[79] To investigate the coupling effect more closely, a glass tip with a diameter of $\sim$1 μm was used to touch the surface of a rolled-up microtube. The purpose was to make a direct interaction with the evanescent field of the resonant wave. Spectral characterizations with and without the tip showed obvious shifts in the resonant wavelengths, and the values were in good agreement with the prediction from perturbation theory.[72,80] Due to the different field distributions of the axial modes (Fig. 1(f)), the modes overlapped with the tip to different extents, leading to different shifts. In addition, shifts could also be observed when the tip was moved perpendicularly to the axis of the tube because the overlaps changed correspondingly.[72] Tuning the resonant wavelength *via* its interaction with the evanescent field is currently used in sensing applications, which will be discussed later in Section 5.

Another important parameter of resonance is the polarization state. In a symmetric microtubular cavity, the resonant wave is linearly polarized and the electrical field is oriented parallel to the tube axis for transverse magnetic (TM) modes.[60] However, recent research showed that in the case of an asymmetric (cone-like) tube, the resonant wave is no longer linearly polarized.[81] As shown in Fig. 2(a), a linear polarization state is composed of the in-phase components of right and left circular polarization: $a(0) = a_{+}(0) + a_{-}(0)$. An asymmetric microtubular resonator, on the contrary, provides a platform to realize spin–orbit coupling of photons, and the right and left circular components acquire a geometric phase with opposite signs: $a = a_{+}e^{-i\varphi} + a_{-}e^{-i\varphi}$, where φ is the geometric phase. As shown in Fig. 2(a), the conversion of amplitudes between the two components leads to a change from a linear to an elliptical polarization.[81] The orientation of the major axis of the polarization is tilted by an angle (equal to the geometric phase φ) with respect to the initial orientation, and this value can be experimentally obtained, as shown in Fig. 2(b) and (c). In the

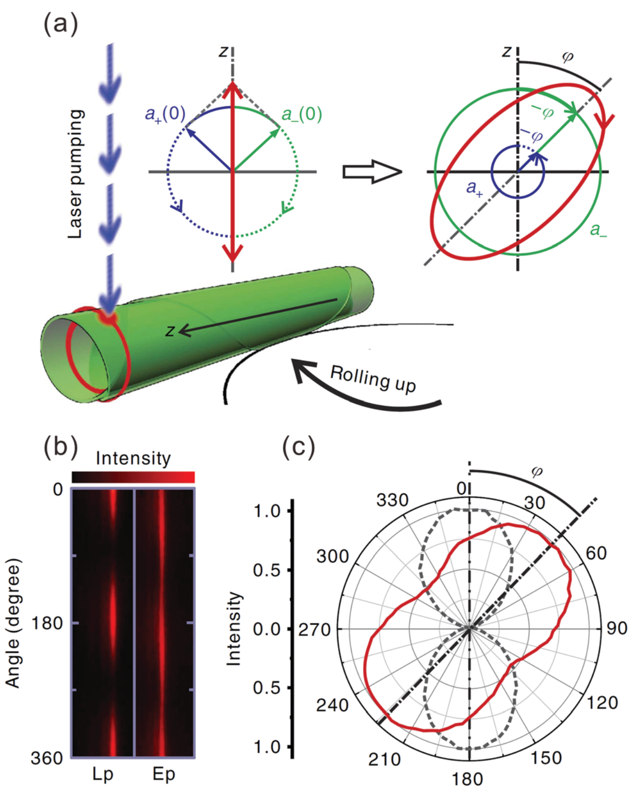

Fig. 2 (a) For resonance in an asymmetric microtubular cavity, the linearly polarized incident wave evolves into an elliptically polarized wave with the major axis tilted out of (with an angle φ) the tube axis. (b) Resonant mode intensity maps of a linear polarization (L_p) state measured from a symmetric tube and an elliptical polarization (E_p) state measured from an asymmetric tube. (c) Corresponding polar diagram. The linear polarization (black dashed line) is parallel to the tube axis while the elliptical polarization exhibits a tilt angle φ with respect to the tube axis. Reprinted from ref. 81.

intensity map from a symmetric microtube (L_P), a linear polarization along the tube axis can be observed (left panel of Fig. 2(b) and black dashed line in Fig. 2(c)). However, in the asymmetric case (E_P in right panel of Fig. 2(b) and red solid line in Fig. 2(c)), the varying but unbroken polarization trace is characteristic of elliptical polarization. This phenomenon reveals the essential physical processes of a non-Abelian evolution, and may have potential applications in the field of on-chip quantum information technologies.[81]

4 Surface plasmon and rolled-up metamaterials

Curvature-dependent localized surface plasmon (LSP) modes from nanostructures made from noble metals have gained increasing attention. By changing the curvature of the nanostructure, the distribution of the electron density can be tuned, leading to alteration of the surface plasmon resonance.[82] This tuning approach can be realized in a rolled-up microtube as the diameter can be well controlled.[53,83] Spectral characterization of microtubes made from noble metals indicates that the excitation of the plasmon mode and local electromagnetic field is greatly enhanced.[82] Theoretical simulation further demonstrates that with decreasing curvature, the intensity of the excited electromagnetic field near the surface decreases, indicating that the excitation efficiency of the plasmon mode is lower.[82]

The surface plasmon can propagate in the ring cross section of a microtube made from a noble metal, in which case it is known as a surface plasmon polariton (SPP). The coupling of a plasmon mode and a photon mode (*e.g.*, the aforementioned WGM of electromagnetic resonance, referred to here as a photon mode for clarity) in microtubular structures was theoretically investigated in 2011.[84] The self-interference of the hybrid plasmon–photon mode led to an azimuthal mode with a Q-factor larger than 100. The intriguingly high Q-factor was believed to be due to the above coupling effect.[84] The coupling phenomenon was later investigated in detail by Yin *et al.*[85,86] in an oxide microtubular cavity coated with a gold cap on the top. In such a cavity, the wave propagates in both the dielectric medium (uncoated bottom part) and the metal/dielectric medium (coated top part). In the bottom part, the wave is confined by the tube wall while in the top part, both the photon mode and the SPP localized at the gold surface exist simultaneously.[85] The resonance with TM or TE (transverse electric polarization, with the electric field perpendicular to the tube axis) polarization was spectrally examined. Prior to coating with Au, both TM and TE modes are photon modes in the oxide and the TM mode is dominant.[60,62,85] After coating, and in contrast to the redshift caused by coating with a dielectric material,[87] the Au layer produces a blueshift for both TM and TE modes, due to the negative permittivity of Au.[85,88] Moreover, the intensity of the TE mode is five times higher than that of the TM mode, indicating an efficient coupling between the TE photon mode and the SPP.[85] In addition to the polarization, a thinner wall was found to play a crucial role in the excitation of the strongly hybridized plasmon–photon mode, because there exists a competition between the confinement of the wave within the wall and the potential barrier introduced by the metal layer.[85,86] The competition leads to three types of hybrid plasmon–photon modes corresponding to fields mostly localized at the inner (weakly hybridized), both inner and outer (moderately hybridized), and outer (strongly hybridized) surface of the metal coating.[86] Correspondingly, a "phase diagram" was presented in ref. 86. For a very thick metal layer, the shielding effect and the absorption loss become significant, which makes the hybrid mode eventually undetectable.[86]

As discussed in Section 2, the microtubular cavity provides both circular and axial confinements of the wave propagation. Recent experimental work shows that coupling should also exist between plasmon and axial photon mode.[89] It was found that a nanogap-confined LSP can effectively couple with the axial mode.[89] The upper-right inset of Fig. 3(a) shows a sketch of an Au coating on a microtubular cavity, in which Au nanogaps can only be present in the top area of the tube and at the edge of the lobe (lower-left inset of Fig. 3(a), denoted "hot arcs"). Although the peak of the LSP resonance at the nanogap is at 0.89 eV, the broad band overlaps with the spectral range of the photon mode (cyan area of Fig. 3(a)). When the positions of the axial mode and hot arc coincide (*i.e.*, the hot arc spatially overlaps with an antinode of the axial mode), strong coupling should cause an obvious shift of the axial mode.[89] As the position of the nanogap can be tuned by changing the orientation angle of the lobe (θ), a selective coupling is achieved. The insets of Fig. 3(b) and (c) show two microtubular cavities with θ of $\sim 90^\circ$ and $\sim 240^\circ$ respectively. Due to their similar geometries, they show almost identical spectra before Au coating (upper panels of Fig. 3(b) and (c)), but a distinct difference can be observed after Au coating (lower panels of Fig. 3(b) and (c)). For $\theta \approx 90^\circ$, the hot arc is located at the center of the lobe, and all modes experience a blueshift while the odd axial modes (E_1, E_3, E_5, *etc.*) exhibit an additional pronounced blueshift (Fig. 3(b)) and enhanced intensity. The phenomenon is ascribed to the large overlap between the hot arc and the odd modes, which have an antinode at the center (see also Fig. 1(f)). However, for $\theta \approx 240^\circ$, the hot arcs are located at the side edges of the lobe and only overlap with the antinodes at the edges, and thus almost identical blueshifts are observed for all axial modes (Fig. 3(c)).

In the rolling process, nanomembranes are closely stacked on top of each other, which represents a novel way to fabricate radial metamaterials consisting of metal/oxide or metal/semiconductor multi-layers with tunable thicknesses and thickness ratios.[90–94] Both theoretical and experimental research demonstrate that the plasma frequency of metamaterials of this kind can be tuned over a broad range by changing their structural parameters, which is in good agreement with the description of metamaterial.[92] It was noticed that the effective permittivity tensor of the metamaterial can be manipulated by altering the thickness ratio of the metal and the semiconductor layers, and microstructures with elliptic or hyperbolic dispersion can be intentionally designed.[90,94] With the help of FDTD simulation, the potentials of these metamaterials as hyper-lenses have

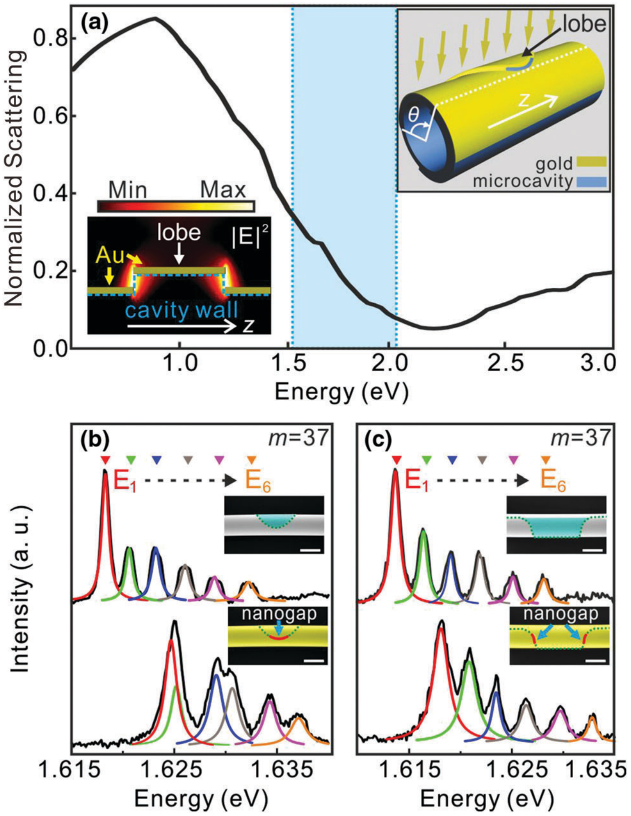

Fig. 3 (a) Calculated resonant spectrum of LSP confined to the Au nanogap. The cyan area is the spectral range of the photon mode. The upper-right inset shows a sketch of the Au layer deposited onto a rolled-up microtubular structure with the lobe orientation angle θ. The lower-left inset shows the LSP supported by the nanogaps at the lobe edge. (b and c) Show axial modes measured before (top panels) and after (bottom panels) Au coating on two rolled-up cavities with $\theta \approx 90°$ and 240° respectively. The colored curves are Lorentzian fits of the individual axial modes identified by the triangular symbols. The insets in (b and c) show the morphologies of the corresponding cavities with the marked hot arcs. The scale bar is 5 μm. Reprinted with permission from ref. 89. Copyright 2016 by the American Physical Society.

been explored: when the wave propagates from the inner to the outer surface, sub-wavelength details can be magnified by the ratio of the outer and the inner radii due to conservation of the angular momentum of the wave vector.[92,95,96] By impedance matching the rolled-up hyper-lens to the surrounding medium, higher transmission is possible and results in a higher resolution.[95] The rolled-up structure also provides convenience in producing metamaterials with quantum wells embedded. In one such structure an enhanced spontaneous emission rate of quantum wells was reported.[90]

3D metamaterials can be designed by considering the unique 3D microtubular structure. For instance, Rottler *et al.*[97] have fabricated a 3D fishnet-type metamaterial consisting of six alternating layers of metal and semiconductor with drilled holes. Experimental results demonstrate that the structure is a single-negative material possessing a negative real part of the refractive index and can be made double-negative by changing the hole size.[97] When the wave propagation along the axial direction in a rolled-up microstructure was taken into consideration, a dual effect of surface plasmon and classical waveguiding therein was theoretically predicted.[91] Recent theoretical[98] and experimental[99] investigations also exhibited the possibility of fabricating 3D photonic crystal structures by rolling pre-patterned nanomembranes, demonstrating a new way of designing and producing 3D metamaterials.

5 Sensing applications

5.1 Sensing based on evanescent interaction

The evanescent wave plays an important role in rolled-up microtubular cavities, especially those with very small wall thicknesses.[62,100] The coupling of the resonance in the micro-cavity and the nearby waveguide *via* evanescent interaction was used to detect the resonant wave in a near-field way and the use of a waveguide has the additional advantage of guiding the electromagnetic wave in a predetermined direction.[49] The interaction/coupling was found to be able to detect resonant modes with high *Q*-factors.[47,101] Coupled devices were previously realized by manually placing a fiber taper in the vicinity of the surface of the microtubular structure[50,71,101–105] or by placing a microtubular structure on a waveguide fabricated by lithography.[101,106] The former suffers from drawbacks of mechanical vibrations, low reproducibility, and system instability while the latter is serial and time-consuming.[107] In order to overcome these deficiencies, researchers recently developed a technique to fully and monolithically integrate rolled-up microtubular structures with waveguides for on-chip coupling.[49,107,108] Fig. 4(a) and (b) show optical microscope images of the rolled-up microtubular structures directly fabricated on a series of waveguides with different lengths.[108] They differ in the fine patterns in the central coupling region: the triangle patterns in Fig. 4(b) are introduced to enhance the axial confinement. Fig. 4(c) shows the experimentally measured transmission spectra for the waveguides with or without microtubes coupled. The blue and the red plots illustrate the spectra of devices I and II in Fig. 4(a) and (b) respectively. Coupling between the waveguides and the microtubes can be clearly identified at discrete wavelengths, and shifted resonant wavelengths are ascribed to the different axial confinements.[108] Compared to the first two approaches, the monolithically integrated device is suitable for mass production and more importantly, provides much more accurate control of the coupling distance, which is crucial for an effective coupling (critical coupling).[46,106,108]

The evanescent interaction between the wave in the micro-tubular resonator and the surrounding materials or structures near the tube wall (both inner and outer region) leads to a shift of the resonant wavelength and thus sensing applications can be realized without any labelling processes.[94] In addition, the cylindrical channel nature of microtubular cavities can inherently combine fluidic functionality with spectral sensitivity.[17] The opto-fluidic devices fabricated have the ability to analyze fluids with volumes in the range of femto-liters.

The first attempt was carried out by inserting an aqueous sugar solution into the microtubular cavity. The change of the

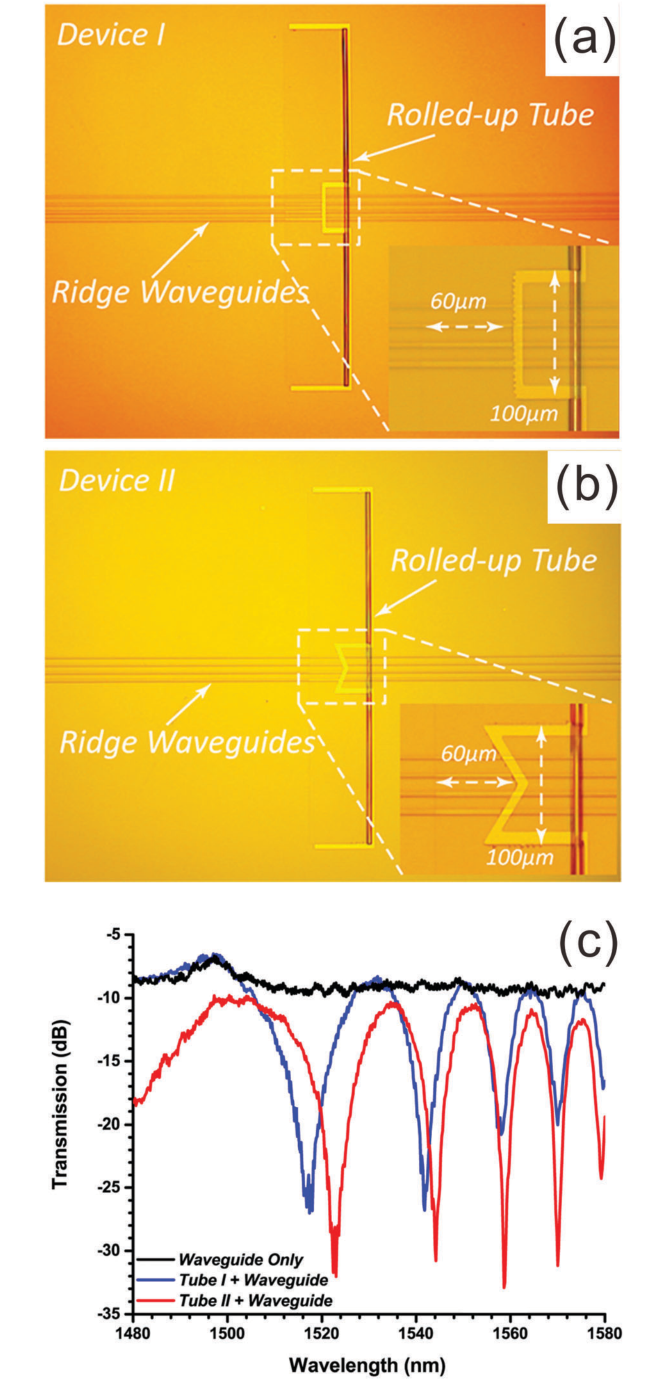

Fig. 4 (a) and (b) Optical microscopy images of the top view of rolled-up microtubes integrated with waveguides. Devices I and II contain different axial patterns in the coupling regions. (c) Transmission spectra of the waveguide only (black), device I (blue), and device II (red). Adapted from ref. 108, with the permission of AIP Publishing.

refractive index of the interior material thus led to a detectable redshift of the WGM.[65] A systematic study concerning the influence of the evanescent interaction on WGMs in microtubular structures was later presented. Polarized spectral characterization demonstrated that both TM and TE resonances are weakened when the microtubular structure is immersed into the liquids because the higher refractive indices of the liquids increase the loss of resonant energy, and the phenomenon is more pronounced in TE modes.[62] Therefore, for a simple means of detection, it has been suggested that the shifts of the TM modes be adopted for sensing. For a WGM with a certain azimuthal number, a redshift was observed by experiment, in good agreement with the theoretical prediction.[62] The sensitivity, defined as $S = \Delta\lambda/\Delta n$, where $\Delta\lambda$ and Δn represent the shift of the mode position and the difference in refractive indices respectively, was determined to be as high as hundreds of nm/RIU (nanometer per refractive index unit).[62] In addition to the spectral shift of the WGM, it was reported that the evanescent interaction between cavity and liquid also influences the resonance along the tube axis: the axial mode spacing is increased due to the deeper axial potential well after liquid filling, which can be used as a new sensing methodology.[109]

Sensing based on evanescent interaction is highly sensitive to the evanescent field emanating from the tube wall, and thus the issue of loss needs to be addressed. The *Q*-factor is essentially determined by the loss of energy, and heavy loss broadens the WGM, resulting in a low *Q*-factor.[55] The corresponding powerful evanescent field can enhance the sensitivity of the structure.[62,110–112] However, in the case of huge loss, the ultra-low *Q*-factor may make the WGM undetectable, so that the detection limit is unacceptably high. Thus, the balance between sensitivity and the detection limit needs to be considered for practical applications. Theoretically, a rolled-up metamaterial tube with infinite medium would have both a high *Q*-factor and high sensitivity.[94] However, for practical use, a coating layer made by atomic layer deposition (ALD) was found to be an effective approach to reconcile these two counteracting tendencies.[62] For any given microtubular device, the larger the azimuthal number of the WGM, the better the confinement of resonant energy in the tube wall, because the intensity of the field has more nodes, which decreases the sensitivity. Operating the device in a longer wavelength range may thus lead to higher sensitivity but a lower *Q*-factor and larger detection limit.[62]

By using the sensing mechanism mentioned above, Harazim *et al.*[42] later fabricated integrated opto-fluidic devices combining the lab-on-a-chip fabrication approach and rolled-up technique, as shown in Fig. 5. The device shows good stability and reproducibility, and real-time sensing ability with a maximum sensitivity of 880 nm per RIU. The approach proposed by this work paves the way for practical applications of integrative rolled-up microtubular structures.

As the evanescent field is strongest at the interface between the wall and surrounding medium, it is expected that the WGM should be particularly sensitive to tiny alterations and modifications in the vicinity of the wall surface.[113–115] This idea has been used to detect molecules adsorbed or deposited on the wall. For instance, the positions of WGMs were found to shift to lower energies when the tube wall was coated with Al_2O_3 monolayers, and the shift due to each Al_2O_3 layer with a thickness of ~0.9 Å was quantitatively determined to be 0.35 meV.[114] More importantly, it was demonstrated that this approach can be used to monitor the dynamic processes of molecule

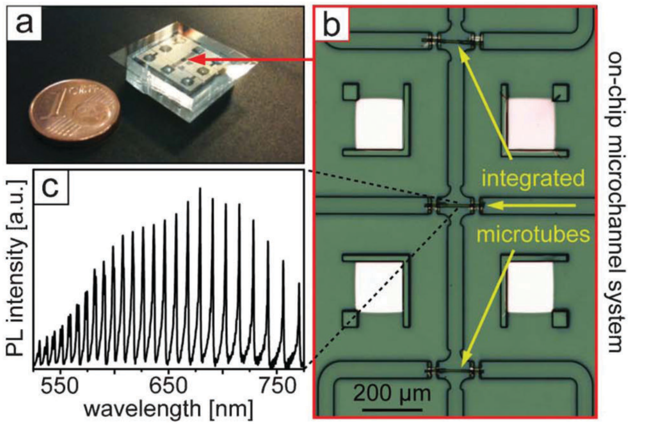

Fig. 5 (a) Photo of an opto-fluidic sensing chip device. (b) Optical microscope image of three microtubular structures integrated into a microchannel system. (c) Photoluminescence spectrum measured on a microtubular structure integrated into the chip. Adapted from ref. 42, with permission from The Royal Society of Chemistry.

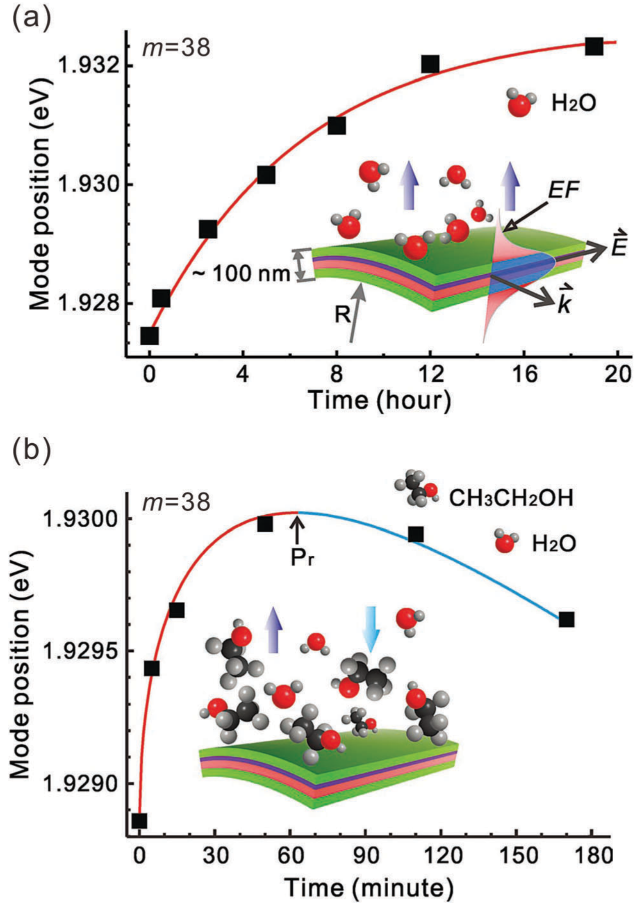

Fig. 6 (a) Dynamic desorption process of H_2O molecules from the tube wall by monitoring the mode (m = 38) position as a function of time. The process is fitted by the LDF model (red curve). The inset shows a diagram of the desorption process. (b) Bi-directional dynamic process of desorption of ethanol molecules and adsorption of H_2O molecules. A turning point is evident at around 60 min. The inset shows a diagram of the desorption/adsorption processes. Adapted with permission from ref. 113.

adsorption/desorption. In the designed experiment, after wetting at ambient conditions, the microtubular structure was transferred into a drying chamber and the resonant positions were recorded, as shown in Fig. 6(a). One can see that the mode gradually blueshifts with time due to the continuous desorption process of H_2O molecules.[113,115] After 19 h, the tube wall is completely dried and the mode position approaches a constant value. The shift process can be well fitted by the linear-driving-force (LDF) model (red solid line in Fig. 6(a)).[113,116] An additional experiment was carried out by dropping ethanol onto the surface of a dried microtube, and a redshift occurred.[113] When the microtube was exposed to the air, the mode position continuously blueshifted in the initial stage, reflecting the desorption of ethanol molecules (Fig. 6(b)).[113] Once the ethanol molecules were desorbed, the vacancies were occupied by H_2O molecules due to their much stronger hydrogen bonding strength, as indicated by a redshift (Fig. 6(b)). The shift shown in Fig. 6(b) indicates a bi-directional dynamic process combining desorption of ethanol molecules and adsorption of H_2O molecules, and a turning point is evident at around 60 min.[113] These results suggest that a microtubular cavity can be used to track the non-equilibrium dynamics of molecular adsorption/desorption.

5.2 Geometry-related sensing

As discussed in Sections 2 and 3, changing the geometrical parameters of a microtubular resonator alters its resonance properties, and this can be employed to detect interactions that lead to deformation of the structure. This methodology is, however, less investigated compared to the use of resonators as evanescent sensors and only a few studies have been presented so far.

As a self-assembly process, the rolling of nanomembranes may cause the formation of nanogaps between the rotations. Theoretical simulation and experimental observation prove that the existence of nanogaps in the tube wall leads to a decrease of the *Q*-factor of the resonator. In a sophisticated experiment carried out by Smith *et al.*,[117] a rolled-up microtube was connected to a microsyringe pump at one end and a living NIH 3T3 fibroblast mouse cell was sucked into the microtube from the opposite opening. The cell exerted an outward force on the tube wall from the inside, which produced a more compact wall by closing the nanogaps. The corresponding lower leakage of resonant energy gave way to a higher *Q*-factor.[117,118] This method may be further developed to investigate the interaction between living cells and 3D scaffolds by using an optical approach.

The sensing can also be performed in a more controllable way. In order to produce a microtubular structure with tunable geometry, an oxide microtube was immersed in a water-sensitive polymer solution to form a sandwiched polymer/oxide/polymer wall.[119] The swelling of the polymer in an environment with high relative humidity (RH) due to diffusion of H_2O molecules into the polymer caused an increase of the wall thickness and a decrease of the wall's refractive index. As a consequence, the WGMs shifted to longer wavelength (see Fig. 7(a)), while for a pure oxide (unmodified) microtube at a

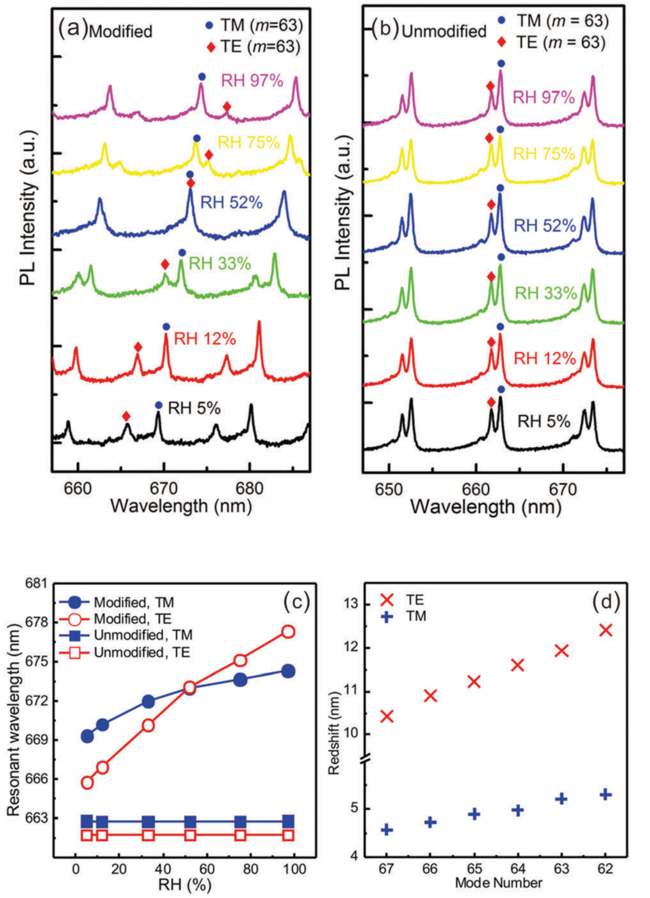

Fig. 7 Photoluminescence spectra of oxide microtube acquired under increasing RH after (a) and before (b) polymer modification. Symbols mark the evolution of TM (circle) and TE (diamond) resonant wavelengths as a function of RH at the azimuthal number m = 63. (c) Resonant wavelengths (azimuthal number m = 63) as a function of RH. The rectangles refer to results obtained from an oxide microtube and the circles are from a modified polymer microtube. The red and blue plots correspond to TE and TM modes, respectively. (d) Dependence of wavelength shift on azimuthal numbers for TE modes (red) and TM modes (blue). The vertical axis represents the accumulated redshift with RH increasing from 5% to 97%. Reproduced from ref. 119, with permission from The Royal Society of Chemistry.

range of humidities, no shift could be detected (Fig. 7(b)). Fig. 7(c) and (d) further demonstrate that the shift of the TE mode corresponds to an average sensitivity (the shift of the mode position corresponding to RH change of 1%) of 130 pm per RH%, which is about 10 times larger than normal WGM-type sensors.[119] In addition, modes with smaller azimuthal numbers demonstrate larger redshifts (Fig. 7(d)), which is ascribed to stronger evanescent interactions with the surrounding medium.[62,119]

5.3 Sensing based on Raman scattering

Surface enhanced Raman scattering (SERS) is a powerful spectroscopy technique that can provide fingerprint, non-destructive, and ultra-sensitive characterization.[120,121] As discussed in Section 4, LSP modes can be excited when a microtube with a noble metal layer in the tube wall is irradiated by optical light of a certain wavelength, and the corresponding enhanced local electromagnetic field will enable SERS.[82,93] Microtubular structures of this kind thus represent excellent candidates for highly sensitive optical sensors.[82]

The sensitivities of SERS-type sensors were found to be determined by the Q-factor of the plasmon resonance, but the intrinsically high ohmic losses of metals result in low Q-factors.[119,122,123] Combining SERS with a resonator has been considered as a method to optimize performance (see also Section 4).[124,125] An attempt to combine a WGM-type microtubular resonator and a surface plasmon for improved SERS sensing was carried out recently, where microtubular cavities with Ag nanoparticles between the rotations were used.[126] Fig. 8(a) shows a scanning electron microscopy (SEM) image of a micro-tubular cavity with a diameter of 850 nm. Three regions, namely Ag nanoparticles arrayed on a flat nanomembrane (left side of the microcavity), the microcavity itself, and a silicon substrate (right side of the microcavity), are clearly shown. Rhodamine solution (R6G, 10^{-5} M), used as a probe chemical, was subsequently deposited and dried in air for the Raman measurement. Detailed Raman spectra at different featured locations along the green arrow in Fig. 8(a) are displayed in Fig. 8(b). On the silicon substrate, no Raman signal can be detected, while Raman spectra of R6G are obtained on the Ag nanoparticle array.[126] This indicates that surface plasmon modes are excited in the Ag nanoparticles and contribute to the enhancement of Raman scattering (*i.e.*, SERS). As for the spectra from the microtubular cavity, the Raman signals are remarkably enhanced, as shown in the red spectra of Fig. 8(b). Such an enhancement suggests that besides the surface plasmon effect of the Ag nanoparticles, the tubular geometry, which supports WGMs, can greatly improve SERS due to a coupling effect.[126] In order to tune the resonant wavelength of the microcavity for effective excitation of the plasmon, a conical microtubular cavity was used in the experiment. As such, each point along the tube axis corresponds to a ring resonator with variable diameter (ranging from 242 to 1030 nm).[126] A linear scan along the tube axis thus can be regarded as an approach to tuning the resonant wavelength. The blue circles in Fig. 8(c) show the Raman intensity detected from R6G molecules of different diameters attached to the conical microtube, and the red curve represents the theoretically calculated average electrical field intensities. Fig. 8(d) further demonstrates the electrical field distribution from theoretical simulation. The size-dependent enhancement shows a series of peaks at diameters of $\sim$500 and 820 nm, and the experimental results fit the calculation/simulation very well.[126] The enhancement at the tube diameter of $\sim$500 nm mainly originates from the resonant mode with azimuthal number m = 3, while the enhancement at the tube diameter of $\sim$820 nm mainly results from the resonant mode with azimuthal number m = 5.[126] This observation proves that the Raman scattering can be greatly enhanced due to the coupling effect at the resonant wavelengths.

Finally, we should stress that Raman enhancement can also be observed from a microtubular structure even when plasmon resonance from a noble metal structure is not present.[126,127] Characterization of a pure dielectric microtube also shows

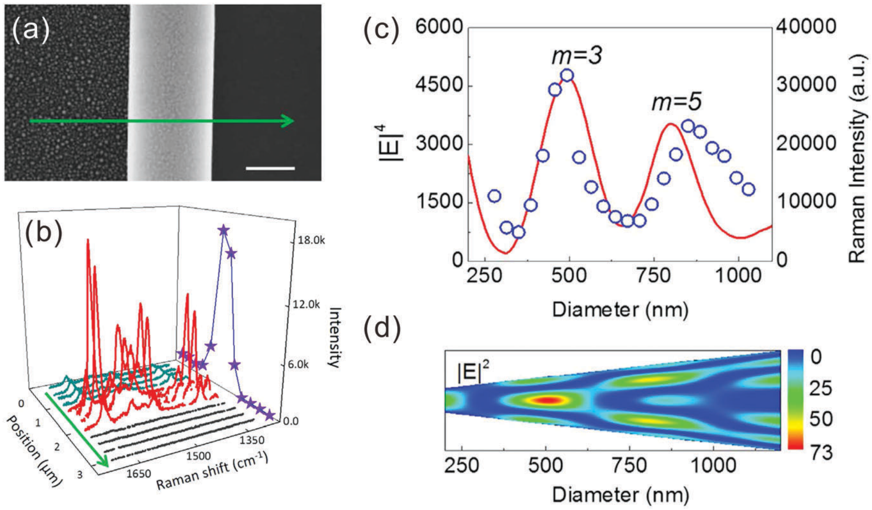

Fig. 8 (a) SEM image of a rolled-up microtube. (b) Raman spectra of the linear scan along the green arrow marked in (a). The blue stars refer to the intensity of the 1650 cm^{-1} band extracted from the spectra. The excitation wavelength is 514.5 nm. (c) Raman enhancement of R6G as a function of tube diameter using a 514.5 nm excitation. The calculated $|E|^4$ (red line) in the tube wall is plotted together with the measured Raman intensity (blue circles). (d) Simulated electrical field distribution in the tube wall of a conical microtube illuminated by a laser of 514.5 nm. Adapted from ref. 126.

amplified Raman scattering due to the efficient coupling of the probe molecules at the non-evanescent regimes of resonance in the rolled-up microtube.[127] The on-resonance of the excitation wavelength and/or shifted Stokes wavelengths were shown to enhance the Raman scattering by a factor of more than 100.[127] This finding may suggest a new type of platform for sensing by Raman scattering given appropriate optimization.

6 Summary and outlook

This review summarized recent research regarding the propagation and resonance of electromagnetic waves in unique rolled-up tubular microcavities. The fabrication of microtubular structures normally combines top-down and bottom-up methods by rolling pre-strained nanomembranes with different geometries. The confinement and propagation of an electromagnetic wave in such a microcavity exhibit 3D characteristics, both in the circular-like cross section and along the longitudinal direction (tube axis). The resonance of the wave is very sensitive to the geometrical parameters and therefore can be easily tuned by altering the geometry of the nanomembrane. The rolling process also provides a convenient way to produce a stack of multilayers made from different materials with tunable thicknesses, demonstrating a new method to prepare 3D metamaterials. The interactions between the microtube and the external environment *via* evanescent interaction or geometrical changes promise interesting sensing applications, such as refractometry and molecule detection, SERS, *etc.*

The future of rolled-up microcavities lies in many aspects from fundamental science to practical applications. The rolled-up technique enables the production of 3D structures from desired materials with designed geometries. The corresponding resonance can thus be tuned in terms of wavelength range and *Q*-factor. Functional materials may also be incorporated to achieve effective coupling between the electromagnetic resonance and other physical fields, giving birth to multi-functional devices with good tunability. Considering the on-chip integratability of rolled-up structures, researchers may also be able to produce a sensing device to realize real-time detection of external interactions. The combination of resonance and other functions on a single device also indicates their application potentials in a "lab-in-a-tube" system.

Acknowledgements

This work was supported by the National Natural Science Foundation of China (No. 51322201, 51475093, and U1632115), Science and Technology Commission of Shanghai Municipality (No. 14JC1400200), and Visiting Scholar Foundation of National Key Laboratory of Fundamental Science of Micro/Nano-Devices and System Technology in Chongqing University (No. 2014MS03).

References

1 http://en.wikipedia.org/wiki/Resonator.
2 P. M. Sousa, V. Chu and J. P. Conde, *J. Appl. Phys.*, 2013, **113**, 134508.
3 A. Hajati, D. Latev, D. Gardner, A. Hajati, D. Imai, M. Torrey and M. Schoeppler, *Appl. Phys. Lett.*, 2012, **101**, 253101.
4 U. Bog, T. Laue, T. Grossmann, T. Beck, T. Wienhold, B. Richter, M. Hirtz, H. Fuchs, H. Kalt and T. Mappes, *Lab Chip*, 2013, **13**, 2701.
5 M. C. Estevez, M. Alvarez and L. M. Lechuga, *Laser Photonics Rev.*, 2012, **6**, 463.
6 H. Jin, J. Zhou, X. L. He, W. B. Wang, H. W. Guo, S. R. Dong, D. M. Wang, Y. Xu, J. F. Geng, J. K. Luo and W. I. Milne, *Sci. Rep.*, 2013, **3**, 2140.

7 B. Svilicic, E. Mastropaolo, B. Flynn and R. Cheung, *IEEE Electron Device Lett.*, 2012, **33**, 278.
8 T. Manzaneque, V. Ruiz-Diez, J. Hernando-García, E. Wistrela, M. Kucera, U. Schmid and J. L. Sáchez-Rojas, *Sens. Actuators, A*, 2014, **220**, 305.
9 C. J. Hood, T. W. Lynn, A. C. Doherty, A. S. Parkins and H. J. Kimble, *Science*, 2000, **287**, 1447.
10 K. J. Vahala, *Nature*, 2003, **424**, 839.
11 S. C. Yang, Y. Wang and H. D. Sun, *Adv. Opt. Mater.*, 2015, **3**, 1136.
12 B. B. Wang, J. G. Ma, L. Wei, J. A. Xu, G. Bi and Z. S. Shi, *Appl. Phys. Lett.*, 2010, **97**, 231103.
13 Z. Q. Li, X. Y. Hu, Y. B. Zhang, Y. L. Fu, H. Yang and Q. H. Gong, *Appl. Phys. Lett.*, 2011, **99**, 141105.
14 D. W. Vernooy, V. S. Ilchenko, H. Mabuchi, E. W. Streed and H. J. Kimble, *Opt. Lett.*, 1998, **23**, 247.
15 B. Guilhabert, C. Foucher, A. M. Haughey, E. Mutlugun, Y. Gao, J. Herrnsdorf, H. D. Sun, H. V. Demir, M. Dawson and N. Laurand, *Opt. Express*, 2014, **22**, 7308.
16 A. B. Matsko and V. S. Ilchenko, *IEEE J. Sel. Top. Quantum Electron.*, 2006, **12**, 3.
17 J. Wang, T. R. Zhan, G. S. Huang, P. K. Chu and Y. F. Mei, *Laser Photonics Rev.*, 2013, **8**, 521.
18 L. Rayleigh, *London, Edinburgh Dublin Philos. Mag. J. Sci.*, 1910, **20**, 1001.
19 L. Rayleigh, *Proc. R. Soc. London, Ser. A*, 1912, **86**, 207.
20 R. D. Richtmyer, *J. Appl. Phys.*, 1939, **10**, 391.
21 C. G. B. Garrett, W. Kaiser and W. L. Bond, *Phys. Rev.*, 1961, **124**, 1807.
22 M. Cai, O. Painter and K. J. Vahala, *Phys. Rev. Lett.*, 2000, **85**, 74.
23 S. Lacey, H. Wang, D. H. Foster and J. U. Nockel, *Phys. Rev. Lett.*, 2003, **91**, 4.
24 J. Ward and O. Benson, *Laser Photonics Rev.*, 2011, **5**, 553.
25 S. L. McCall, A. F. J. Levi, R. E. Slusher, S. J. Pearton and R. A. Logan, *Appl. Phys. Lett.*, 1992, **60**, 289.
26 W. Bogaerts, P. De Heyn, T. Van Vaerenbergh, K. De Vos, S. K. Selvaraja, T. Claes, P. Dumon, P. Bienstman, D. Van Thourhout and R. Baets, *Laser Photonics Rev.*, 2012, **6**, 47.
27 S. Feng, T. Lei, H. Chen, H. Cai, X. Luo and A. W. Poon, *Laser Photonics Rev.*, 2012, **6**, 145.
28 D. K. Armani, T. J. Kippenberg, S. M. Spillane and K. J. Vahala, *Nature*, 2003, **421**, 925.
29 K. Padmaraju and K. Bergman, *Nanophotonics*, 2014, **3**, 269.
30 T. Beck, S. Schloer, T. Grossmann, T. Mappes and H. Kalt, *Opt. Express*, 2012, **20**, 22012.
31 L. Shang, L. Liu and L. Xu, *Appl. Phys. Lett.*, 2008, **92**, 071111.
32 G. Kakarantzas, T. E. Dimmick, T. A. Birks, R. Le Roux and P. S. J. Russell, *Opt. Lett.*, 2001, **26**, 1137.
33 M. Pöllinger, D. O'Shea, F. Warken and A. Rauschenbeutel, *Phys. Rev. Lett.*, 2009, **103**, 053901.
34 M. Sumetsky, Y. Dulashko and R. S. Windeler, *Opt. Lett.*, 2010, **35**, 898.
35 A. Watkins, J. Ward, Y. Wu and S. Nic Chormaic, *Opt. Lett.*, 2011, **36**, 2113.
36 B. E. Little, S. T. Chu, H. A. Haus, J. Foresi and J. P. Laine, *J. Lightwave Technol.*, 1997, **15**, 998.
37 D. O'Shea, J. Ward, B. Shortt and S. Nic Chormaic, *IEEE Photonics Technol. Lett.*, 2007, **19**, 1720.
38 Y. Wu, J. M. Ward and S. Nic Chormaic, *J. Appl. Phys.*, 2010, **107**, 033103.
39 J. M. Ward, N. Dhasmana and S. N. Chormaic, *Eur. Phys. J.: Spec. Top.*, 2014, **223**, 1917.
40 F. Vollmer and L. Yang, *Nanophotonics*, 2012, **1**, 267.
41 M.-S. Kwon and W. H. Steier, *Opt. Express*, 2008, **16**, 9372.
42 S. M. Harazim, V. A. Bolanos Quinones, S. Kiravittaya, S. Sanchez and O. Schmidt, *Lab Chip*, 2012, **12**, 2649.
43 S. I. Shopova, I. M. White, Y. Sun, H. Zhu, X. Fan, G. Frye-Mason, A. Thompson and S.-J. Ja, *Anal. Chem.*, 2008, **80**, 2232.
44 H. Y. Zhu, I. M. White, J. D. Suter, M. Zourob and X. D. Fan, *Anal. Chem.*, 2007, **79**, 930.
45 H. Y. Zhu, I. M. White, J. D. Suter and X. D. Fan, *Biosens. Bioelectron.*, 2008, **24**, 461.
46 Y. L. Li, Y. F. Fang, J. Wang, L. Wang, S. W. Tang, C. P. Jiang, L. R. Zheng and Y. F. Mei, *Lab Chip*, 2016, **16**, 4406.
47 X. Yu, L. L. Goddard, X. L. Li and X. G. Chen, *Appl. Phys. Lett.*, 2016, **109**, 111104.
48 X. Yu, E. Arbabi, L. L. Goddard, X. L. Li and X. G. Chen, *Appl. Phys. Lett.*, 2015, **107**, 031102.
49 S. Böttner, M. R. Jorgensen and O. G. Schmidt, *Scr. Mater.*, 2016, **122**, 119.
50 S. Böttner, S. L. Li, M. R. Jorgensen and O. G. Schmidt, *Appl. Phys. Lett.*, 2013, **102**, 251119.
51 V. Ya Prinz, V. A. Seleznev, A. K. Gutakovsky, A. V. Chehovskiy, V. V. Preobrazhenskii, M. A. Putyato and T. A. Gavrilova, *Physica E*, 2000, **6**, 828.
52 O. G. Schmidt and K. Eberl, *Nature*, 2001, **410**, 168.
53 Y. F. Mei, G. S. Huang, A. A. Solovev, E. Bermudez-Urena, I. Mönch, F. Ding, T. Reindl, R. K. Y. Fu, P. K. Chu and O. G. Schmidt, *Adv. Mater.*, 2008, **20**, 4085.
54 X. L. Li, *Adv. Opt. Photonics*, 2011, **3**, 366.
55 T. Kipp, H. Welsch, Ch. Strelow, Ch. Heyn and D. Heitmann, *Phys. Rev. Lett.*, 2006, **96**, 077403.
56 F. Li, Z. T. Mi and S. Vicknesh, *Opt. Lett.*, 2009, **34**, 2915.
57 F. Li and Z. T. Mi, *Opt. Express*, 2009, **17**, 19933.
58 Ch. Strelow, H. Rehberg, C. M. Schultz, H. Welsch, Ch. Heyn, D. Heitmann and T. Kipp, *Phys. Rev. Lett.*, 2008, **101**, 127403.
59 Ch. Strelow, C. M. Schultz, H. Rehberg, H. Welsch, Ch. Heyn, D. Heitmann and T. Kipp, *Phys. Rev. B: Condens. Matter Mater. Phys.*, 2007, **76**, 045303.
60 G. S. Huang, S. Kiravittaya, V. A. Bolaños Quiñones, F. Ding, M. Benyoucef, A. Rastelli, Y. F. Mei and O. G. Schmidt, *Appl. Phys. Lett.*, 2009, **94**, 141901.
61 M. H. T. Dastjerdi, M. Djavid, S. Arafin, X. Liu, P. Bianucci, Z. Mi and P. J. Poole, *Semicond. Sci. Technol.*, 2013, **28**, 094007.
62 G. S. Huang, V. A. Bolaños Quiñones, F. Ding, S. Kiravittaya, Y. F. Mei and O. G. Schmidt, *ACS Nano*, 2010, **4**, 3123.

63 F. Y. Zhao, T. R. Zhan, G. S. Huang, Y. F. Mei and X. H. Hu, *Lab Chip*, 2012, **12**, 3798.
64 J. Wang, T. R. Zhan, G. S. Huang, X. G. Cui, X. H. Hu and Y. F. Mei, *Opt. Express*, 2012, **20**, 18555.
65 A. Bernardi, S. Kiravittaya, A. Rastelli, R. Songmuang, D. J. Thurmer, M. Benyoucef and O. G. Schmidt, *Appl. Phys. Lett.*, 2008, **93**, 094106.
66 M. Hosoda and T. Shigaki, *Appl. Phys. Lett.*, 2007, **90**, 181107.
67 Y. F. Fang, S. L. Li and Y. F. Mei, *Phys. Rev. A*, 2016, **94**, 033804.
68 H. Cao and J. Wiersig, *Rev. Mod. Phys.*, 2015, **87**, 61.
69 C. Strelow, C. M. Schultz, H. Rehberg, M. Sauer, H. Welsch, A. Stemmann, C. Heyn, D. Heitmann and T. Kipp, *Phys. Rev. B: Condens. Matter Mater. Phys.*, 2012, **85**, 155329.
70 Z. T. Mi and P. Bianucci, *Curr. Opin. Solid State Mater. Sci.*, 2012, **16**, 52.
71 A. Madani, S. Böttner, M. R. Jorgensen and O. G. Schmidt, *Opt. Lett.*, 2014, **39**, 189.
72 S. L. Li, L. B. Ma, H. L. Zhen, M. R. Jorgensen, S. Kiravittaya and O. G. Schmidt, *Appl. Phys. Lett.*, 2012, **101**, 231106.
73 K. Dietrich, C. Strelow, C. Schliehe, C. Hyn, A. Stemmann, S. Schwaiger, S. Mendach, A. Mews, H. Weller, D. Heitmsnn and T. Kipp, *Nano Lett.*, 2010, **10**, 627.
74 H. Wang, H. L. Zhen, S. L. Li, Y. L. Jing, G. S. Huang, Y. F. Mei and W. Lu, *Sci. Adv.*, 2016, **2**, e1600027.
75 V. A. Bolaños Quiñones, L. B. Ma, S. L. Li, M. Jorgensen, S. Kiravittaya and O. G. Schmidt, *Opt. Lett.*, 2012, **37**, 4284.
76 Y. W. Lan, S. L. Li, Z. Y. Cai, Y. F. Mei and S. Kiravittaya, *Opt. Commun.*, 2017, **386**, 72.
77 S. D. Miao, D. C. Chen, A. Madani, M. R. Jorgensen, V. A. Bolaños Quiñones, L. B. Ma, S. G. Hickey, A. Eychmüller and O. G. Schmidt, *Adv. Opt. Mater.*, 2015, **3**, 187.
78 A. Madani, L. B. Ma, S. D. Miao, M. R. Jorgensen and O. G. Schmidt, *Nanoscale*, 2016, **8**, 9498.
79 A. Madani, V. A. Bolaños Quiñones, L. B. Ma, S. D. Miao, M. R. Jorgensen and O. G. Schmidt, *Appl. Phys. Lett.*, 2016, **108**, 171105.
80 S. G. Johnson, M. Ibanescu, M. A. Skorobogatiy, O. Weisberg, J. D. Joannopoulos and Y. Fink, *Phys. Rev. E: Stat., Nonlinear, Soft Matter Phys.*, 2002, **65**, 066611.
81 L. B. Ma, S. L. Li, V. M. Fomin, M. Hentschel, J. B. Götte, Y. Yin, M. R. Jorgensen and O. G. Schmidt, *Nat. Commun.*, 2016, **7**, 10983.
82 Y. Yin, T. Qiu, L. B. Ma, X. Z. Lang, Y. Zhang, G. S. Huang, Y. F. Mei and O. G. Schmidt, *J. Phys. Chem. C*, 2012, **116**, 25504.
83 C. Deneke, C. Muller, N. Y. Jin-Phillipp and O. G. Schmidt, *Semicond. Sci. Technol.*, 2002, **17**, 1278.
84 A. Rottler, M. Bröll, S. Schwaiger, D. Heitmann and S. Mendach, *Opt. Lett.*, 2011, **36**, 1240.
85 Y. Yin, S. L. Li, S. Giudicatti, C. Y. Jiang, L. B. Ma and O. G. Schmidt, *Phys. Rev. B: Condens. Matter Mater. Phys.*, 2015, **92**, 241403(R).
86 Y. Yin, S. L. Li, V. Engemaier, S. Giudicatti, E. S. G. Naz, L. B. Ma and O. G. Schmidt, *Phys. Rev. A*, 2016, **94**, 013832.
87 L. B. Ma, S. Kiravittaya, V. A. Bolaños Quiñones, S. L. Li, Y. F. Mei and O. G. Schmidt, *Opt. Lett.*, 2011, **36**, 3840.
88 A. Rottler, M. Harland, M. Bröll, M. Klingbeil, J. Ehlermann and S. Mendach, *Phys. Rev. Lett.*, 2013, **111**, 253901.
89 Y. Yin, S. L. Li, S. Böttner, F. F. Yuan, S. Giudicatti, E. S. G. Naz, L. B. Ma and O. G. Schmidt, *Phys. Rev. Lett.*, 2016, **116**, 253904.
90 K. Marvin Schulz, H. Vu, S. Schwaiger, A. Rottler, T. Korn, D. Sonnenberg, T. Kipp and S. Mendach, *Phys. Rev. Lett.*, 2016, **117**, 085503.
91 E. J. Smith, Z. Liu, Y. F. Mei and O. G. Schmidt, *Nano Lett.*, 2010, **10**, 1.
92 S. Schwaiger, M. Bröll, A. Krohn, A. Stemmann, C. Heyn, Y. Stark, D. Stickler, D. Heitmann and S. Mendach, *Phys. Rev. Lett.*, 2009, **102**, 163903.
93 Y. Zhang, D. Han, D. Y. Du, G. S. Huang, T. Qiu and Y. F. Mei, *Plasmonics*, 2015, **10**, 949.
94 S. W. Tang, Y. F. Fang, Z. W. Liu, L. Zhou and Y. F. Mei, *Lab Chip*, 2016, **16**, 182.
95 E. J. Smith, Z. Liu, Y. F. Mei and O. G. Schmidt, *Appl. Phys. Lett.*, 2009, **95**, 083104.
96 X. Jacob, L. V. Alekseyev and E. Narimanov, *Opt. Express*, 2006, **14**, 8247.
97 A. Rottler, M. Harland, M. Bröll, S. Schwaiger, D. Stickler, A. Stemmann, C. Heyn, D. Heitmann and S. Mendach, *Appl. Phys. Lett.*, 2012, **100**, 151104.
98 M. R. Jorgensen, S. Giudicatti and O. G. Schmidt, *Phys. Rev. Lett.*, 2013, **87**, 041803(R).
99 L. A. Ibbotson and J. J. Baumberg, *Nanotechnology*, 2013, **24**, 305301.
100 S. Sedaghat and A. Zarifkar, *Opt. Commun.*, 2017, **382**, 167.
101 Z. Tian, V. Veerasubramanian, P. Bianucci, S. Mukherjee, Z. Mi, A. G. Kirk and D. V. Plant, *Opt. Express*, 2011, **19**, 12164.
102 Q. Zhong, Z. Tian, M. H. T. Dastjerdi, Z. Mi and D. V. Plant, *Opt. Express*, 2013, **21**, 18909.
103 Z. Tian, V. Veerasubramanian, P. Bianucci, Z. Mi, A. G. Kirk and D. V. Plant, *Opt. Lett.*, 2011, **36**, 3506.
104 S. Böttner, S. L. Li, M. R. Jorgensen and O. G. Schmidt, *Appl. Phys. Lett.*, 2014, **105**, 121106.
105 Q. Zhong, Z. Tian, M. H. T. Dastjerdi, Z. Mi and D. V. Plant, *IEEE Photonics Technol. Lett.*, 2013, **25**, 1691.
106 Q. Zhong, Z. Tian, V. Veerasubramanian, M. H. T. Dastjerdi, Z. Mi and D. V. Plant, *Opt. Lett.*, 2014, **39**, 2699.
107 A. Madani, M. Klieinert, D. Stolarek, L. Zimmermann, L. B. Ma and O. G. Schmidt, *Opt. Lett.*, 2015, **40**, 3826.
108 X. Yu, E. Arbabi, L. L. Goddard, X. L. Li and X. G. Chen, *Appl. Phys. Lett.*, 2015, **107**, 031102.
109 V. A. Bolaños Quiñones, L. B. Ma, S. L. Li, M. Jorgensen, S. Kiravittaya and O. G. Schmidt, *Appl. Phys. Lett.*, 2012, **101**, 151107.
110 H. Zhu, I. M. White, J. D. Suter, P. S. Dale and X. Fan, *Opt. Express*, 2007, **15**, 9139.
111 M. Sumetsky, R. S. Windeler, Y. Dulashko and X. Fan, *Opt. Express*, 2007, **15**, 14376.
112 J. Trommer, S. Böttner, S. L. Li, S. Kiravittaya, M. R. Jorgensen and O. G. Schmidt, *Opt. Lett.*, 2014, **39**, 6335.

113 L. B. Ma, S. L. Li, V. A. Bolaños Quiñones, L. C. Yang, W. Xi, M. Jorgensen, S. Baunack, Y. F. Mei, S. Kiravittaya and O. G. Schmidt, *Adv. Mater.*, 2013, **25**, 2357.
114 V. A. Bolaños Quiñones, G. S. Huang, J. D. Plumhof, S. Kiravittaya, A. Rastelli, Y. F. Mei and O. G. Schmidt, *Opt. Lett.*, 2009, **34**, 2315.
115 J. Zhong, J. Wang, G. S. Huang, G. L. Yuan and Y. F. Mei, *Nanoscale Res. Lett.*, 2013, **8**, 530.
116 C. R. Reid and K. M. Thomas, *Langmuir*, 1999, **15**, 3206.
117 E. J. Smith, S. Schulze, S. Kiravittaya, Y. F. Mei, S. Sanchez and O. G. Schmidt, *Nano Lett.*, 2011, **11**, 4037.
118 S. Böttner, S. L. Li, J. Trommer, S. Kiravittaya and O. G. Schmidt, *Opt. Lett.*, 2012, **37**, 5136.
119 J. Zhang, J. Zhong, Y. F. Fang, J. Wang, G. S. Huang, X. G. Cui and Y. F. Mei, *Nanoscale*, 2014, **6**, 13646.
120 S. M. Nie and S. R. Emery, *Science*, 1997, **275**, 1102.
121 Y. C. Cao, R. Jin and C. A. Mirkin, *Science*, 2002, **297**, 1536.
122 X.-M. Qian and S. M. Nie, *Chem. Soc. Rev.*, 2008, **37**, 912.
123 E. C. Le Ru, E. Blackie, M. Meyer and P. G. Etchegoin, *J. Phys. Chem. C*, 2007, **111**, 13794.
124 Y. Guo, M. K. Khaing Oo, K. Reddy and X. Fan, *ACS Nano*, 2012, **6**, 381.
125 I. M. White, J. Gohring and X. Fan, *Opt. Express*, 2007, **15**, 17433.
126 J. Zhang, J. X. Li, S. W. Tang, Y. F. Fang, J. Wang, G. S. Huang, R. Liu, L. R. Zheng, X. G. Cui and Y. F. Mei, *Sci. Rep.*, 2015, **5**, 15012.
127 X. Y. Lin, Y. F. Fang, L. J. Zhu, J. Zhang, G. S. Huang, J. Wang and Y. F. Mei, *Adv. Opt. Mater.*, 2016, **4**, 936.